ELSEVIER

Journal of Power Sources 81–82 (1999) 1–7

JOURNAL OF POWER SOURCES

www.elsevier.com/locate/jpowsour

Advanced carbon anode materials for lithium ion cells

Hideto Azuma *, Hiroshi Imoto, Shin'ichiro Yamada, Koji Sekai

Research Center, Sony Corporation, 174 Fujitsuka-cho, Hodogaya-ku, Yokohama 240, Japan

Abstract

Three kinds of carbon have been used for commercial cells: graphite, soft carbon and hard carbon. The difference in the structures of these three kinds of carbon is shown clearly using our new model for soft and hard carbon structure. The lithium-doped state of these three kinds of carbon is discussed using the new structural model and published ^{7}Li NMR data. A large reversible capacity is demonstrated in the hard carbons derived from some vegetable fibers. Two mechanisms—one enhancing the adsorbing force of pseudo-metallic lithium atoms and one reducing the repulsion force between doped lithium atoms—which together produce a high reversible capacity, are explained.

Keywords: Lithium-ion cell; Anode; Hard carbon; Structural analysis; Graphite; Soft carbon

1. Introduction

Three kinds of carbon have been used for commercial cells: graphite, soft carbon and hard carbon. Graphite intercalates up to a maximum of one lithium atom per six carbon atoms under ambient conditions [1,2]. Many soft carbons show a maximum reversible capacity when heat-treated around 1200°C of about 300 mAh/g [3]. Lithium can be doped to some hard carbons up to over one carbon atom per six carbon atoms. From early reports [4,5] of 400 mAh/g of rechargeable capacity, improvement of reversible capacity without an increase of irreversible capacity has been attempted and over 500 mAh/g of reversible capacity with a small irreversible capacity of about 60 mAh/g has been achieved [6]. The relation between structure and performance as an anode, and the mechanism of lithium insertion have also been studied [7,8]. These studies have increased our knowledge of lithium-doped hard carbon, but the structural model used in these studies was basically the model proposed by Franklin in 1951 [9]. In this paper, the difference in the structure and the lithium-doped state of these three kinds of carbon is discussed in terms of a new model for soft and hard carbon structure.

2. Structure of graphite, soft carbon and hard carbon

Graphite is a three-dimensional ordered crystal (Fig. 1). Soft carbon and hard carbon constructed with two-dimensional ordered graphene sheets which are randomly stacked [10] have a 'turbostratic' structure. Soft carbon is called a graphitizing carbon because it is graphitized by heat treatment over 2000°C. On the other hand, hard carbon is never graphitized, even at 3000°C under ambient pressure, so it is called a non-graphitizing carbon. The raw material usually determines whether the carbon obtained is soft or hard. Typical raw materials for soft carbon are petroleum pitch and coal tar pitch. Acenaphtylene can be used in the laboratory as a substitute for pitch. Hard carbon can be obtained by heat treating thermosetting resins such as phenolic resin, and vegetable fibers such as coconut shell. Soft carbons and hard carbons heat treated at 1000 to 1400°C, purified natural graphite and artificial graphite have been used for the anodes of lithium ion cells. Some carbon materials heat treated under around 800°C have a large capacity, but their discharging potential is too high for them to be used in current cells because the voltage of the cell will be lower than 3 V. The lithium-doping mechanism of these carbon materials is different from the mechanism under consideration here [11].

* Corresponding author. Tel.: +81-45-353-6857; Fax: +81-45-353-6910; E-mail: hazuma@src.sony.co.jp

0378-7753/99/$ - see front matter
PII: S0378-7753(99)00122-6

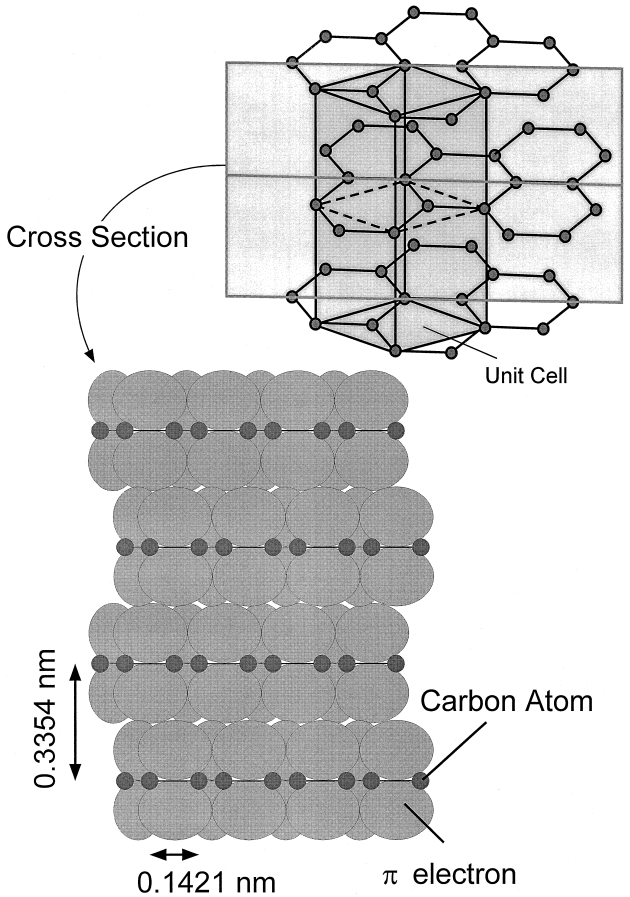

Fig. 1. Structure of hexagonal graphite showing ABAB stacking. Schematic of cross-section of stacking layers considering the thickness of each carbon layer is also shown.

Before discussing our new structural model, we will first comment on the density of the three kinds of carbon materials. The X-ray density of graphite crystal is 2.26 g/cm^3 and soft carbon, e.g., coke, has about 2.0 g/cm^3 true density. Hard carbon can have a density between 1.4 and 1.8 g/cm^3 and its density value can depend on the measuring method. For example, the density of phenolic resin carbon (whose HTT (heat treatment temperature) is 1100°C) is about 1.45 g/cm^3 when measured with a pycnometer using *n*-butyl alcohol, but is about 2.0 g/cm^3 when measured with a pycnometer using He gas displacement. This suggests that there are small pores into which He atoms can diffuse but which the molecules of *n*-butyl alcohol cannot enter. Based on the density measured using *n*-butyl alcohol, we calculated the average interlayer distance of the carbons. Table 1 shows the calculated interlayer distance of soft carbon and hard carbon.

The structure of soft and hard carbon is recognized to be as in Fig. 2a [9]. This is the structural model proposed by Franklin. It seems that soft and hard carbon heat treated at around 1000°C has received abundant attention for over 40 years. Franklin's model is useful to depict structural properties in an easy-to-understand way, but it is difficult

Table 1
Typical density of soft carbon and hard carbon and their calculated average interlayer distance

	ρ (density) [g cm^{-3}]	d_a^a (nm)
Graphite (standard)	2.26	0.3354
Soft carbon	2.02	0.375
Hard carbon	1.45	0.523

[a] d_a: average interlayer distance. Calculated from $d_a = 2.26 \times 3.354/\rho$. Acenaphtylene carbon (soft, HTT 1100°C) and phenolic resin carbon (hard, HTT 1100°C) are used for example.

and inaccurate to calculate diffraction intensity using Franklin's model. Past calculations of diffraction intensity have been thought to be based on the Franklin model on the randomly oriented layers shown in Fig. 2a, but in fact past calculations have been based on the isolated-layer structure shown in Fig. 2b. To show the difference between 'randomly oriented' and 'isolated', we plot in Fig. 2c the density of carbon atoms projected to the thin line in Fig. 2b. The result is solid line in Fig. 2c. If there were any other layers around the isolated layer in Fig. 2b, the broken curve in Fig. 2c should be added to the density plot.

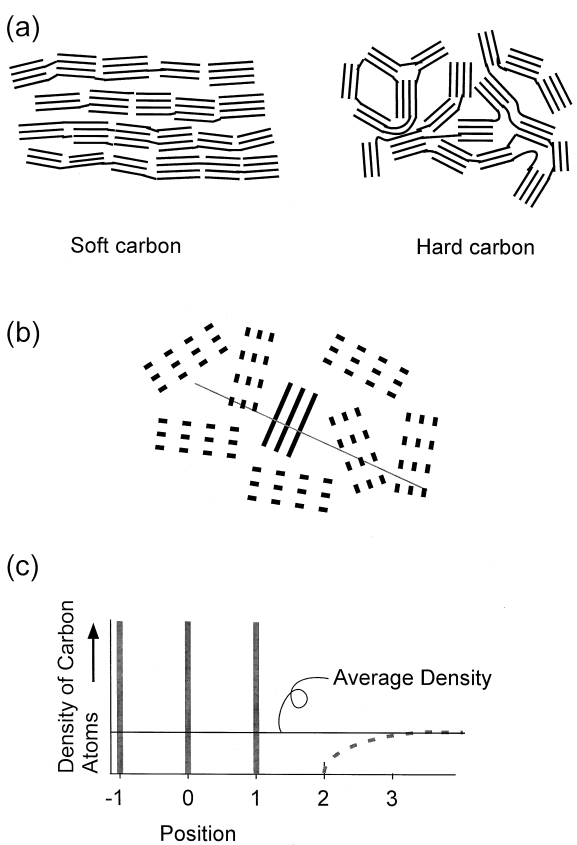

Fig. 2. Conventional structure model for soft and hard carbon and the problem with this model. (a) stacking arrangement models by Franklin [9]. The problem exists in that we have calculated the diffraction intensity not from the model (a) but from an isolated layer (b). The plot of the density of carbon atom (c) projected to the thin line in (b). If we consider the existence of another layers, the broken curve must be added to the plot.

It can be understood by Fourier-transform of the obtained X-ray intensity that the distribution of carbon atoms is as the solid curve in Fig. 3a. The broken curve in Fig. 3a is derived from the mistaken structure shown in Fig. 2b and the resulting solid lines in Fig. 2c. We have proposed a model which assumes a nearest-neighbor interlayer relation [12] and well reproduces the solid curve. The nearest-neighbor interlayer relation takes two forms—a relatively well-stacked layer and a not well-stacked layer (see Fig. 3b). The essential characteristic of our model is the recognition that the interlayer relation has two forms. Our new model has yields diffraction intensity which agrees well with the observed X-ray diffraction intensity (see Fig. 4).

2.1. Soft carbon

Fig. 5a shows that the intralayer carbon–carbon distance in soft and hard carbon is slightly smaller than in graphite and that the carbon atoms are irregularly positioned. In this figure, we use a rounded rectangle with a height of 0.344 nm to represent graphene sheets in cross-section. 0.344 nm is the interlayer distance of turbostatic carbon, which is the typical interlayer distance of non-graphitic carbon. The stacking arrangement of soft carbon is illustrated in Fig. 5b and c, in which the analytic result is for the Acenaphtylene carbon. The length of the rectangle denotes half of the defect-free length: $L_a/2$. L_a is 2.4 nm in this case. 72% of the layers are parallel stacked with an interlayer distance of 0.342 nm and the remaining 28% are not parallel stacked with an interlayer distance of 0.446 nm. Standard deviation (2σ) of the interlayer distance for the not-parallel-stacked layers is 0.20 nm. The average interlayer distance is 0.371 ± 0.004 nm, which almost agrees with Table 1. This estimate suggests that soft carbon has few pores. The consequent total two-dimensional schematic is as in Fig. 5c.

We performed structural analysis on several soft carbon samples of HTT around 200°C, and obtained almost the same results as above. We think that the existence of parallel and not-parallel stacking and the no-pore structure is a characteristic common to all soft carbon.

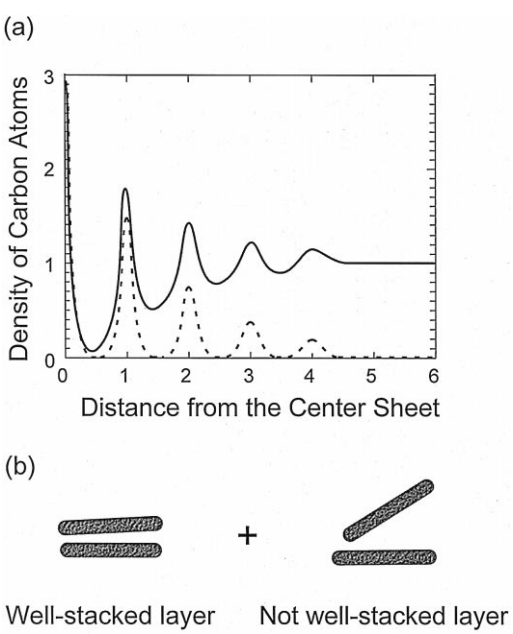

Fig. 3. The density of carbon atoms in non-graphitic carbon projected to the line perpendicular to the center sheet can be plotted as the solid curve in (a). Notice that the broken curve expresses the isolated layers in (b). The solid curve can be reproduced by the new model that assumes a nearest-neighbor interlayer relation which takes two forms—a relatively well-stacked layer and a not well-stacked layer, as shown in (b) [12].

2.2. Hard carbon

For the same sample in Table 1, the structure of carbonized phenolic resin (Psm4436 from Gun'ei Chemical, novolac-type resin) heat treated at 1100°C is illustrated in Fig. 6. The resin was cured with 10% hexametylenediamine at 160°C before heat treatment. The cross-section of graphene sheet is the same as soft carbon, in this case $L_a = 2.1$ nm, so a rectangle 1.0 nm long is used to represent the graphene sheet. There is no parallel-stacking arrangement in hard carbon. There are two forms of interlayer relation, one (45%) 0.343 nm with 0.09 nm of 2σ and the other (55%) 0.47 nm with 0.25 nm of 2σ (Fig. 6a). The form with the shorter interlayer distance has an interlayer distance near that of turbostatic carbon, 0.344 nm. An interlayer distance near that of turbostatic carbon seems to be common in hard carbon. The average interlayer distance is 0.42 nm. This value is much smaller than the calculated interlayer distance in Table 1, but the difference is explained by the existence of pores, as noted previously. The total two-dimensional schematic of phenolic resin carbon is shown in Fig. 6b.

3. Structure providing a large reversible capacity

The reversible capacity of graphite materials can be raised b improving the materials crystallinity. For soft carbon, reversible capacity and charge–discharge efficiency are well balanced when the soft carbon is heat-treated at around 1200°C, and these properties are little influenced by the raw material used. For hard carbon, good performance is obtained when crystallinity is low and it has many small pores [7,13]. In our model, low crystallinity is expressed as a large deviation in interlayer distance. We think that a large deviation in interlayer distance is a requirement for a large reversible capacity. On the other hand, we are not sure whether a smaller pore size contributes an increased reversible capacity or not. We are now investigating the possibility of other structural properties' influencing the performance of the carbon-anode material.

4. The lithium-doped state

We discuss here the lithium-doped state in view of published ^{7}Li NMR [14–16] data. The significance of the Knight shift is first reviewed [17]. ^{7}Li nucleus is subjected to a 261 ppm higher magnetic field in the metallic state than in the ionic state (Li in LiCl is usually used for standard). Pauli paramagnetism of a 2S-like conduction orbital emphasizes the magnetic field at the nucleus. Pauli magnetization is much smaller than usual Curie magnetization, and is almost independent of temperature. The amount of Pauli magnetization is equal to Curie magnetization at Fermi temperature: T_F, which is 5.5×10^4 K for Lithium metal, so the Pauli paramagnet is smaller than $1/100$ of Curie paramagnet at room temperature. The shift of the resonance field due to hyperfine contact between conduction electrons and the nucleus is called the Knight shift.

Knight Shift K is described by Pauli susceptibility χ_s, conduction electron density at the nucleus $|\phi(0)|^2$ and conduction electron density N as $K \propto \chi_s |\phi(0)|^2/N$, where $\chi_s \propto N/T_F$. Consequently, we obtain

$$K \propto |\phi(0)|^2/T_F. \quad (1)$$

When lithium is intercalated in graphite, lithium is partially ionized. $|\phi(0)|^2 = 0$ for Li^+, so $K = 0$ in perfectly ionized case. In the partially ionized case, determining K is impossible unless the orbital ϕ is known. Here, we assume that the orbital does not change and $|\phi(0)|^2$ is reduced in proportion to the degree of progression of the

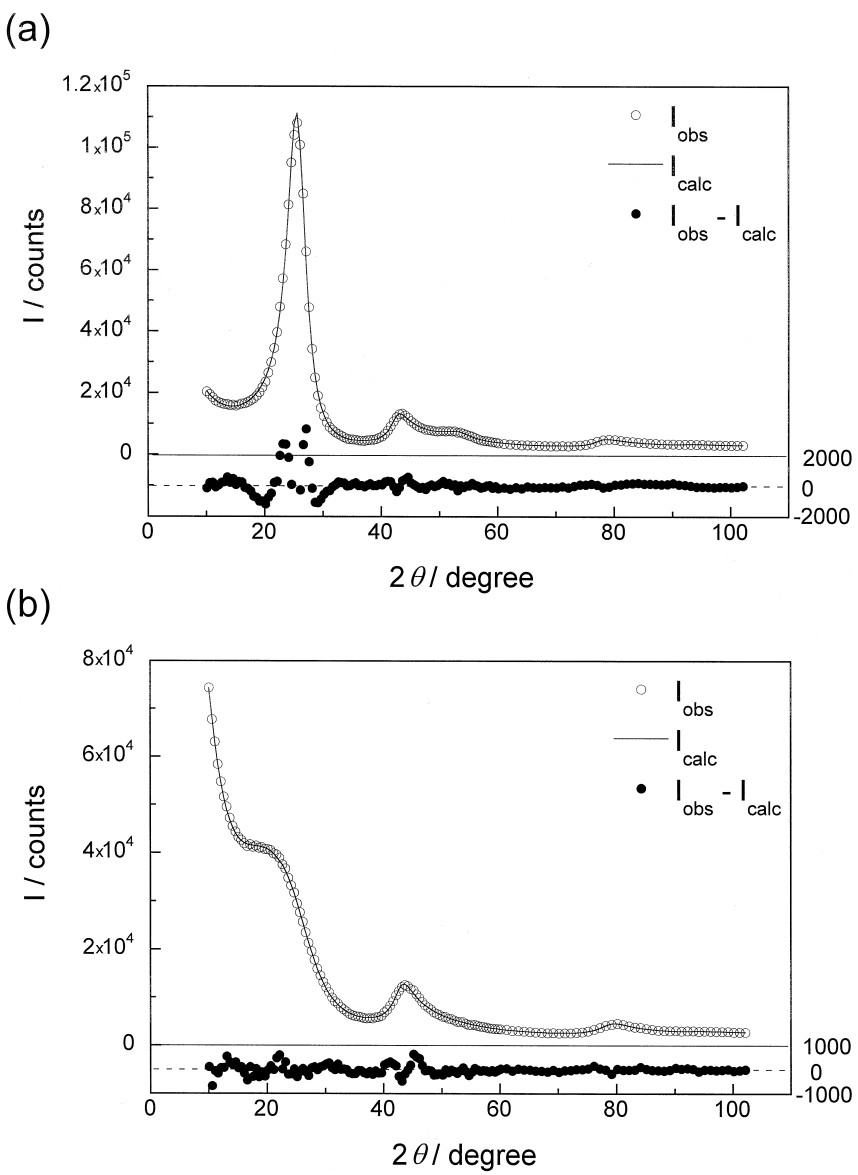

Fig. 4. The observed X-ray diffraction profile and the calculated intensity using our new model to fit the observed intensity. (a) for acenaphtylene carbon and (b) for phenoric resin carbon. In both cases, heat-treatment temperature was 1100°C.

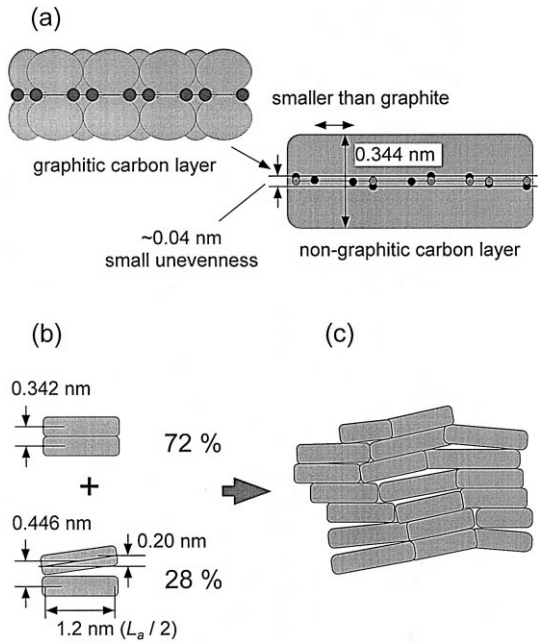

Fig. 5. Stacking arrangement for soft carbon obtained from fitting the calculation in Fig. 4a. (a) Schematic of a graphene sheet in soft and hard carbon heat treated around 1000°C. (b) Stacking arrangement of an acenaphtylene carbon (HTT 1100°C). (c) A two-dimensional structure based on (b).

ionic state. If this assumption is granted, in a state of lower conductive electron density than that of Lithium metal as in a Li-graphite compound, Fermi temperature is reduced, and it can be seen from Eq. (1) that the Knight shift is enlarged. In the case of free electron approximation, Fermi temperature is proportional to electron density to the $2/3$ power, so we obtain

$$K \propto |\phi(0)|^2 N^{-2/3}. \quad (2)$$

4.1. Graphite

The structure of lithium intercalated graphite has been investigated in detail by Ohzuku et al. [1]. The schematic structure of fully lithium-intercalated graphite (C_6Li) can be illustrated as in Fig. 7a and b [18]. Doped lithium can be regarded as being in an almost ionic state based on the ^{7}Li NMR result. The observed 40 ppm of Knight shift [16] can be regarded as being due to the small amount of electrons in the 2S-like valence orbital of lithium. The degree of ionized state is not clear because the 2S-like orbital of lithium metal and that of C_6Li have a different form, and their consequent Pauli susceptibility is different each other as so cannot be compared. If δ electrons remain on lithium, a carbon atom in graphite can accept a maximum of $(1-\delta)/6$ electrons. In C_6Li, the electron source is lithium and the volume per lithium atom is reduced to 0.36 times of that of lithium metal. If the 2S orbital does not change and the free electron model is assumed, using Eq. (2),

$$\delta = 0.36^{2/3} \times 40/261 \cong 0.08.$$

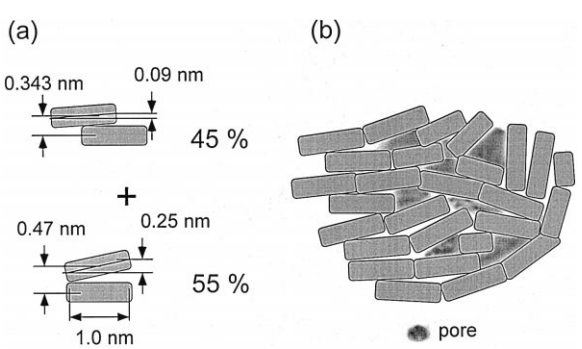

Fig. 6. Stacking arrangement for hard carbon obtained from fitting calculation in Fig. 4b. Same as (b) and (c) of Fig. 5 except the schematics are for a phenoric resin carbon (HTT 1100°C).

4.2. Soft carbon

Soft carbons heat-treated at 1100–1200°C have about 300 mAh/g of reversible capacity. There are no pores in soft carbon, so the structure of lithium doped soft carbon can be illustrated as Fig. 7c. Although a 25 ppm Knight shift is observed [16], it is difficult to understand the mechanism of shift because soft carbon is not crystal. Considering that the electron density in soft carbon is lower than that in graphite, lithium in soft carbon must be

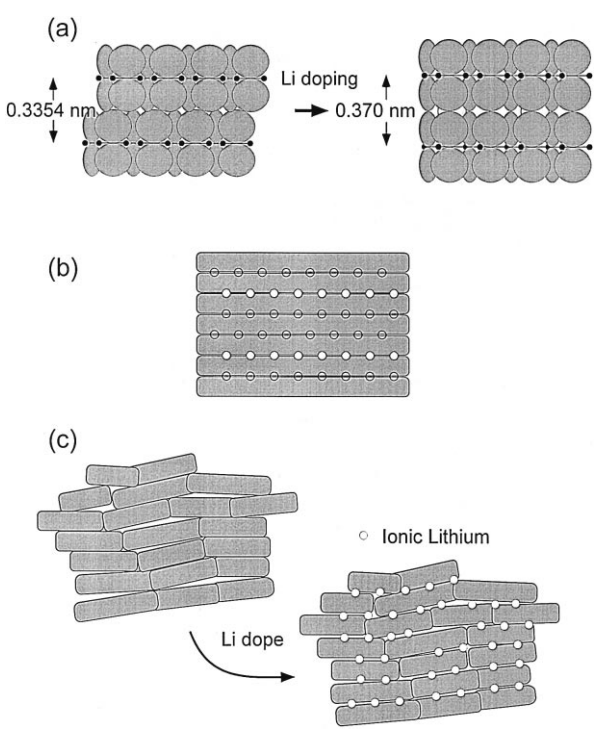

Fig. 7. Structural model of lithium doped (a) graphite [18] and (c) soft carbon. For graphite, an illustration in the same scale as soft carbon is shown in (b). All lithium atoms are depicted as in the ionic state.

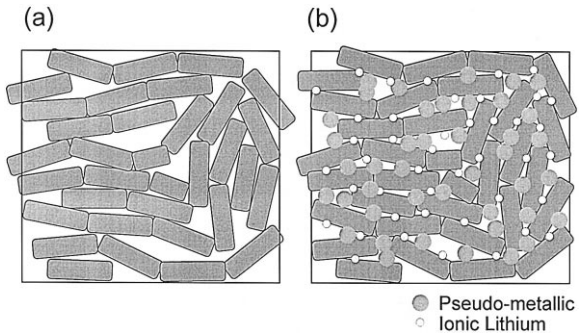

Fig. 8. A possible structural model of lithium-doped hard carbon. (a) A stacking arrangement consistent with density (see Table 1) and with Fig. 6. (b) Ionic and pseudo-metallic lithium arranged in (a).

in an almost fully ionic state. A carbon atom in soft carbon can receive a maximum of 1/7.5 electrons.

4.3. Hard carbon

With charging up to 200 mAh/g, lithium in hard carbon must be in an almost ionic state because the Knight shift observed in hard carbon behaves the same as that in soft carbon. The large Knight shift (over 100 ppm) observed in an over 200 mAh/g charged state [14] suggests that the degree of progression of the ionic state is advanced. The NMR absorption peak corresponding to this large shift splits into two peaks, one around 20 ppm and the other around 200 ppm, in temperatures lower than about 240 K [15]. We think that the 20 ppm peak corresponds to the ionic state and the 200 ppm peak corresponds to the pseudo-metallic state. Data showing that lithium diffusion velocity in lithium metal is equal to the inverse of transverse relaxation time at 230 K [19] suggest the following. Lithium in hard carbon can be categorized into an ionic state and a pseudo-metallic state at low temperatures, but these states cannot be distinguished a temperature higher than about 240 K. We conclude that in hard carbon, lithium doping progresses accompanied by lithium-to-carbon charge transfer until 200 mAh/g of lithium is doped, but subsequently, lithium doping progresses with little charge transfer.

The mechanism of doping a large amount of lithium to hard carbon is complicated. First, the pseudo-metallic state of lithium reduces the repulsion force among the doped lithium atoms. Second, pseudo-metallic lithium can be doped because some enhanced adsorptive force is present in the small gap between graphene sheets as in Fig. 6a. This second phenomenon is analogous to micropore filling. In micropores whose width is under 2 nm, physical adsorption of gas molecules is enhanced by the overlapped surface field (micropore filling) and the adsorptive molecules behave as if they were under high pressure [20]. In order to adsorb the pseudo-metallic lithium, a gap narrower than 2 nm is needed. We can imagine a structure whose interlayer distance—0.523 nm—is shown in Table 1 and Fig. 6 to have carbon layers to have ionic and pseudo-metallic lithium carbon layers arranged as in Fig. 8. In the small gaps shown in Fig. 8b, the pressure which the adsorptive lithium is subjected to may reach that in the condition in which C_2Li is produced [21]. In this situation, in hard carbon we can expect three times the reversible capacity than that of soft carbon, 900 mAh/g.

5. Improvement of hard carbon performance

We previously reported that high-performance hard carbon can be obtained from vegetable fiber such as coffee beans [6]. New high-performance carbon of our recent investigation which was nearly 600 mAh/g of reversible capacity with about 100 mAh/g of irreversible capacity [22] was also obtained from vegetable fiber. According to reports on high-capacity hard carbon, for example, carbon from dewatered sugar [23], saccharide is good raw material.

6. Summary

The difference between the structure of soft carbon and hard carbon is shown, considering their true density and using a model derived from the nearest-neighbor relation. The special properties of hard carbon are that it has no parallel stacking arrangement, and that pseudo-metallic lithium can be doped.

References

[1] T. Ohzuku, Y. Iwakoshi, K. Sawai, J. Electrochem. Soc. 140 (1993) 2490.
[2] J.R. Dahn, Phys. Rev. B 44 (1991) 9170.
[3] N. Takami, A. Satoh, T. Ohsaki, M. Kanda, Electrochim. Acta 42 (1997) 2537.
[4] H. Azuma, A. Omaru, H. Imoto, Y. Nishi, Electrochem. Soc. Japan. Spring Meeting, Abstract 2F10, 1991, p. 157.
[5] H. Imoto, A. Omaru, H. Azuma, Y. Nishi, Electrochem. Soc., 182th Fall Meeting Abstract, 1992, p. 35.
[6] S. Yamada, H. Imoto, K. Sekai, M. Nagamine, Electrochem. Soc. 191st Meeting Extended Abstract, 1997, p. 85.
[7] H. Imoto, M. Nagamine, Y. Nishi, PV 94-28, The Electrochemical Proceedings Series Pennington, NJ, 1995, p. 43.
[8] Y. Liu, J.S. Xue, T. Zheng, J.R. Dahn, Carbon 34 (1996) 193.
[9] R.E. Franklin, Proc. Roy. Soc. A 209 (1951) 196.
[10] B.E. Warren, J. Chem. Phys. 9 (1934) 551.
[11] T. Zheng, Y. Liu, E.W. Fuller, S. Tseng, U. von Sacken, J.R. Dahn, J. Electrochem. Soc. 142 (1995) 2581.
[12] H. Azuma, J. Appl. Cryst. 31 (1998) 910.
[13] W. Xing, J.S. Xue, T. Zheng, A. Gibaud, J.R. Dahn, J. Electrochem. Soc. 143 (1996) 3482.
[14] K. Tatsumi, T. Kawamura, S. Higuchi, H. Hosotubo, H. Nakajima, Y. Sawada, J. Power Sources 68 (1997) 263.
[15] T. Kawamura, T. Hosotubo, K. Tatsumi, Y. Sawada, The 37th Battery Symposium in Japan, Tokyo, Abstract 2A09, 1996, p. 127.
[16] K. Tatsumi, T. Akai, T. Imamura, K. Zaghib, N. Iwashita, S. Higuchi, Y. Sawada, J. Electrochem. Soc. 143 (1996) 1923.

[17] C. Kittel, Introduction to Solid State Physics, 5th edn., Chaps. 14 and 16, Wiley, New York, 1976.
[18] D. Guérard, A. Hérold, Carbon 13 (1975) 337.
[19] H.S. Gutowsky, B.R. McGarve, J. Chem. Phys. 20 (1952) 1472.
[20] J. Imai, M. Souma, S. Ozeki, T. Suzuki, K. Kaneko, J. Phys. Chem. 95 (1991) 9955.
[21] V.A. Nalimova, D. Guerard, M. Lelaurain, O.V. Fateev, Carbon 33 (1995) 177.
[22] H. Imoto et al., to be presented in IBA meeting, 1998.
[23] W. Xing, J.S. Xue, J.R. Dahn, J. Electrochem. Soc. 143 (1996) 3046.